



Cite this: *Nanoscale*, 2015, 7, 11401

## The role of the interface in germanium quantum dots: when not only size matters for quantum confinement effects†‡

S. Cosentino,<sup>\*a</sup> A. M. Mio,<sup>b</sup> E. G. Barbagiovanni,<sup>a</sup> R. Raciti,<sup>a</sup> R. Bahariqushchi,<sup>c</sup> M. Miritello,<sup>a</sup> G. Nicotra,<sup>b</sup> A. Aydinli,<sup>c</sup> C. Spinella,<sup>b</sup> A. Terrasi<sup>a</sup> and S. Mirabella<sup>a</sup>

Quantum confinement (QC) typically assumes a sharp interface between a nanostructure and its environment, leading to an abrupt change in the potential for confined electrons and holes. When the interface is not ideally sharp and clean, significant deviations from the QC rule appear and other parameters beyond the nanostructure size play a considerable role. In this work we elucidate the role of the interface on QC in Ge quantum dots (QDs) synthesized by rf-magnetron sputtering or plasma enhanced chemical vapor deposition (PECVD). Through a detailed electron energy loss spectroscopy (EELS) analysis we investigated the structural and chemical properties of QD interfaces. PECVD QDs exhibit a sharper interface compared to sputter ones, which also evidences a larger contribution of mixed Ge-oxide states. Such a difference strongly modifies the QC strength, as experimentally verified by light absorption spectroscopy. A large size-tuning of the optical bandgap and an increase in the oscillator strength occur when the interface is sharp. A spatially dependent effective mass (SPDEM) model is employed to account for the interface difference between Ge QDs, pointing out a larger reduction in the exciton effective mass in the sharper interface case. These results add new insights into the role of interfaces on confined systems, and open the route for reliable exploitation of QC effects.

Received 6th March 2015,  
Accepted 15th May 2015

DOI: 10.1039/c5nr01480h

www.rsc.org/nanoscale

## Introduction

Quantum confinement in semiconductor nanostructures has attracted much attention in the past decade for the optimization of solar energy harvesting through bandgap modulation and for the development of novel high-efficiency devices.<sup>1</sup> In particular, tunable light absorption and emission in Si and Ge quantum dots (QDs) attracted significant interest for the devel-

opment of solar cells,<sup>2,3</sup> energy-tunable photodetectors,<sup>4–6</sup> optical modulators<sup>7</sup> and optoelectronic devices.<sup>1,8</sup>

Despite the recent progress in fabrication of nanostructure-based devices, a complete understanding and reliable control of the quantum confinement effects (QCE) occurring in semiconductor nanostructures are still under debate, even if they are often ascribed to the nanostructure size only.<sup>9–11</sup> When nanostructure dimensions become smaller than the exciton Bohr radius ( $r_B$ ,  $\sim 5$  nm in Si and  $\sim 24$  nm in Ge<sup>12</sup>), the bandgap ( $E_g$ ) widens and the oscillator strength ( $O_s$ ) increases due to stronger overlapping of electron–hole wave-functions.<sup>9</sup> Many relevant papers emphasized that nanostructure size matters.<sup>10,11,13</sup> Still, it seems to be not the only parameter driving QCE, whereby, a real understanding of the interplay with an interface role is often underrated.<sup>14</sup> This led to contrasting results in the literature, as even when the QD size is fixed, different QCE (in terms of  $E_g$  and/or  $O_s$ ) appear. Several studies demonstrated how the optical properties of Si nanostructures can be varied by solely managing the nanostructure shape,<sup>15</sup> the QD crystalline structure,<sup>16,17</sup> or the potential barriers surrounding the QD.<sup>18–20</sup> Even though a multilayered-nanostructure approach and an appropriate surface passivation could allow an efficient control of QCE *via* size-tuning only,<sup>13</sup> the optical properties of confined systems can be

<sup>a</sup>MATIS IMM-CNR and Dipartimento di Fisica e Astronomia, Università di Catania, via S. Sofia 64, 95123 Catania, Italy. E-mail: salvatore.cosentino@ct.infn.it

<sup>b</sup>IMM-CNR, VII strada 5, 95121 Catania, Italy

<sup>c</sup>Department of Physics, Bilkent University, 06800 Ankara, Turkey

†SC contributed to sample processing, characterization, data analysis and interpretation, and drafted the manuscript. AMM performed STEM and EELS analysis, together with data interpretation. EGB contributed to data interpretation and conceived SPDEM model. RR contributed to sample characterization, data analysis and interpretation. RB and AA provided PECVD samples. MM synthesized sputter samples. GN and CS provided STEM and EELS analysis facilities and helped in data interpretation. AT and SM conceived the study, coordinated the work, contributed to data interpretation and revised the manuscript. All authors read and approved the final manuscript.

‡Electronic supplementary information (ESI) available. See DOI: 10.1039/c5nr01480h

strongly affected by the structural quality of QDs, particularly regarding the effects of the interface.<sup>14,21</sup> Recently, Mariotti *et al.* highlighted the aspects related to the interplay between quantum confinement and surface effects in Si nanocrystals (nc), concluding that: “major gaps between theoretical results and experimental evidence still need to be overcome in order to provide a coherent understanding of Si-nc behaviour and properties”.<sup>14</sup>

An even more puzzling scenario appears for the optical properties of Ge nanostructures. Takeoka *et al.* observed a clear size-dependence of the near infrared photoluminescence from Ge nanocrystals embedded in the SiO<sub>2</sub> matrix due to QCE.<sup>22</sup> Zacharias *et al.* reported on a similar system with a broad size-independent blue-PL emission not attributable to the radiative recombination of the confined excitons, but rather to the contribution of defects at the nanocrystal/matrix interface or in the matrix.<sup>23</sup> A similar behavior holds for light absorption, whereby, Bostedt *et al.* reported on strong QCE in the conduction band of Ge QDs in SiO<sub>2</sub> observed by X-ray absorption spectroscopy.<sup>24</sup> In previous studies, we also experimentally observed that the stoichiometric quality and type of the matrix surrounding the QDs can modify the QCE occurring in these systems.<sup>4,25</sup> In particular, the amount of defects at the QD interface strongly modifies the size-dependent variation of  $E_g$ , which cannot be solely modelled through the standard effective mass approximation (EMA) theory.<sup>4,26,27</sup>

In addition, both theoretical and experimental studies suggest a reduction of the effective mass (EM) in confined structures with respect to the bulk values.<sup>28–30</sup> Still, the QD dimension as well as the matrix–nanostructure interface play paramount roles in the modification of EM. Very recently, a reduction of the carrier EM was experimentally observed for Si nanocrystals embedded in oxide and nitride matrices by EELS analysis.<sup>29</sup> Given the abrupt change in electronic potential occurring at the interface, a suitable model is needed to describe the QCE on EM. Barbagioanni *et al.* proposed a spatially dependent effective mass approximation (SPDEM) model as a correction of the standard EMA to describe the influence of the interface in the bandgap of Si and Ge QDs.<sup>26</sup> Thus, it is clear that a reliable control of QC in QDs requires a deeper investigation of what occurs at the interface, in terms of bonds and defects, and it is essential to disentangle the role of the size from interface effects, if any, and identify the extent of each contribution.

For these reasons, in this work we focus on the interface of Ge QDs in SiO<sub>2</sub> and their interplay in the confinement effects occurring in the light absorption process. By comparing Ge QDs grown by PECVD or sputter techniques, we demonstrate how a different interface can largely modify the size-dependent tuning of the bandgap and oscillator strength. We explain our results through the SPDEM-modified EMA model, shedding new light on the role of a QD–matrix interface, which in essence reveals its key role in building the confinement potential for excitons. These results open the way for a reliable control of QCE and their exploitation for future nanostructure-based devices.

## Experimental

Ge QDs in the SiO<sub>2</sub> matrix were synthesized through the deposition of Ge-rich silicon dioxide thin films (hereafter denoted: SiGeO) by PECVD or rf-magnetron sputtering on quartz or Si substrates. Post-deposition thermal annealing under a N<sub>2</sub> atmosphere induced the nucleation and growth of Ge QDs.<sup>27</sup> The Ge concentrations in the SiGeO films were varied by controlling the rf power of the Ge target (for sputter) or the flux of the precursor gas (GeH<sub>4</sub>, for PECVD). The atomic composition of SiGeO films was measured by Rutherford Backscattering Spectrometry (RBS). Details on the SiGeO deposition, Ge diffusion, QD growth and structural order of Ge QDs are given in ref. 4, 25, 33. The presence and the size distribution of Ge QDs were evaluated by cross sectional transmission electron microscopy in scanning mode (STEM) analysis.

Low-loss electron energy loss spectroscopy (EELS) analysis and high angle annular dark field (HAADF) micrography were performed on individual Ge QDs in SiO<sub>2</sub>, using a sub-angstrom ARM200F STEM operated at 60 kV in order to reduce the beam damage on samples. The instrument was equipped with a probe-corrected C-FEG, able to reach an energy resolution of 0.35 eV, and a GIF Quantum ER for EELS. The probe convergence semiangle was 30 mrad and the collection semiangle was set to 53 mrad in order to minimize the acquisition time and maximize the signal to noise ratio.

SiGeO films were thinned by a standard cross-sectional technique and mechanical polishing followed by Ar<sup>+</sup> ion milling at 2.5 keV (Gatan PIPS). The uniform thickness of the TEM lamella was estimated through STEM-EELS measurement. The thickness of the lamella was estimated through STEM-EELS by the log-ratio method,<sup>34</sup> which gives the thickness in units of total mean free path for all inelastic scattering ( $\lambda$ ). In order to obtain an absolute measurement we considered only regions inside the SiO<sub>2</sub> matrix in which the value of  $\lambda$  is well known. The measurement was repeated in several regions of the TEM lamella for both samples, in order to quantify any possible thickness variation. For both the PECVD and sputter samples we quantified a mean thickness of  $35 \pm 5$  nm. All the STEM-EELS measurements were performed by using the Gatan STEM EELS spectrum imaging (SI) tool in regions of the sample where the QDs do not overlap each other, in particular EELS line-scan acquisitions were performed across the core, interface and matrix region of two individual QDs having a similar dimension. The SI tool moves the probe systematically along the sample over a selected region of interest and the resulting EELS spectra are collected in a data box pixel-by-pixel, allowing advanced spectral post-processing to be performed for every pixel. Every single EELS spectrum had an energy resolution of 0.7 eV FWHM, 1.1 Å probe size, 50 pA of electron beam current, 20 ms of acquisition time, and the pixel size was  $0.1 \times 0.1$  nm<sup>2</sup>. The interface thickness of PECVD and sputter Ge QDs was calculated through a line-scan analysis of high resolution HAADF STEM micrographs using the Z-contrast signal variation across the dia-

meter of a single QD in SiO<sub>2</sub>. This approach was repeated for several QDs with a size in the 3–7 nm range (Fig. 1S of the ESI†).

The optical absorption spectra were determined by combining the transmittance and reflectance of SiGeO thin films deposited on quartz, acquired using a Varian Cary 500 double-beam scanning UV/visible/NIR spectrophotometer, as described in ref. 20, 25.

## Results and discussion

Fig. 1 shows HAADF STEM micrographs of Ge QDs obtained by sputter (a) and PECVD (b) techniques. The ripening phenomenon leading to a size increase with annealing temperature and time is well studied.<sup>20,25,31,32</sup> Therefore, we performed different annealing processes to get comparable ranges of the QD size. Both sets of films evidenced a highly inter-connected array of small Ge QDs, visible as bright spots in Fig. 1. Raman and RBS analysis confirmed that most QDs are amorphous and only a limited fraction of Ge out-diffuses after annealing.<sup>25,33</sup> Table 1 summarizes the values of the Ge atomic concentration ( $C_{\text{Ge}}$ , from RBS analysis), QD size ( $D$ ) and QD concentration (from STEM analysis) in SiGeO films. In order to give a suitable comparison between the two synthesis techniques, the Ge concentration was varied between  $\sim 6.0 \times 10^{21}$  at  $\text{cm}^{-3}$  and  $\sim 1.3 \times 10^{22}$  at  $\text{cm}^{-3}$  for both sets of SiGeO

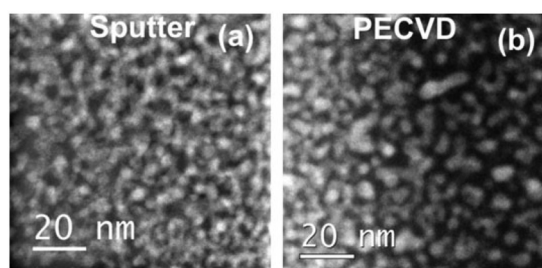


**Fig. 1** Typical cross sectional HAADF STEM images of Ge QDs in SiO<sub>2</sub>. Bright spots correspond to Ge QDs obtained by sputter (a) or PECVD techniques (b) from SiGeO films having  $\sim 1.3 \times 10^{22}$  at  $\text{cm}^{-3}$  of Ge.

**Table 1** Ge concentration of SiGeO films, mean size and concentration of Ge QDs obtained by sputter or PECVD techniques, respectively. The error bar in the QD size is referred to the size distribution

Synthesis technique	Ge concentration, $C_{\text{Ge}}$ [at $\text{cm}^{-3}$ ]	QD size, $D$ [nm]	QD concentration [QD per $\text{cm}^3$ ]
Sputter 600 °C annealing	$5.5 \times 10^{21}$	$2 \pm 0.5$	$1.2 \times 10^{19}$
	$6.0 \times 10^{21}$	$2.5 \pm 0.5$	$7.2 \times 10^{18}$
	$1.15 \times 10^{22}$	$3 \pm 0.5$	$1.3 \times 10^{19}$
	$1.25 \times 10^{22}$	$4 \pm 0.5$	$6.8 \times 10^{18}$
PECVD 800 °C annealing	$7 \times 10^{21}$	$3.5 \pm 1$	$1.4 \times 10^{19}$
	$1.1 \times 10^{22}$	$4.4 \pm 0.7$	$7.6 \times 10^{18}$
	$1.3 \times 10^{22}$	$8.4 \pm 2$	$9.1 \times 10^{17}$

films. Thermal annealing induced the nucleation of small QDs with a mean size in the 2–4 nm range for sputter and 3–10 nm for PECVD SiGeO films. The slightly larger dimensions possessed by PECVD QDs are related to the different kinetics for QD nucleation among PECVD or sputter matrices.<sup>25</sup> Moreover, by considering the QD mean size and the atomic excess concentration of Ge in the SiGeO film, we can estimate the average QD concentration in both PECVD and sputter samples. Both techniques allow the formation of a large amount of QDs after annealing, with typical concentrations of the order of  $10^{18}$ – $10^{19}$  QD per  $\text{cm}^3$ . This value corresponds to a typical mean distance of about 3 nm between the surfaces of two adjacent QDs, which is in agreement with the QD distributions shown in Fig. 1.

In order to provide a comprehensive structural and chemical analysis of the QD interface, we performed a detailed investigation by the low-loss (5–70 eV region) EELS technique, moving from the matrix to the core region of the single QD (Fig. 2). We accurately selected regions of the SiGeO films where QD size distribution was comparable. Moreover, we chose QDs not smaller than 4–5 nm to minimise any resolu-

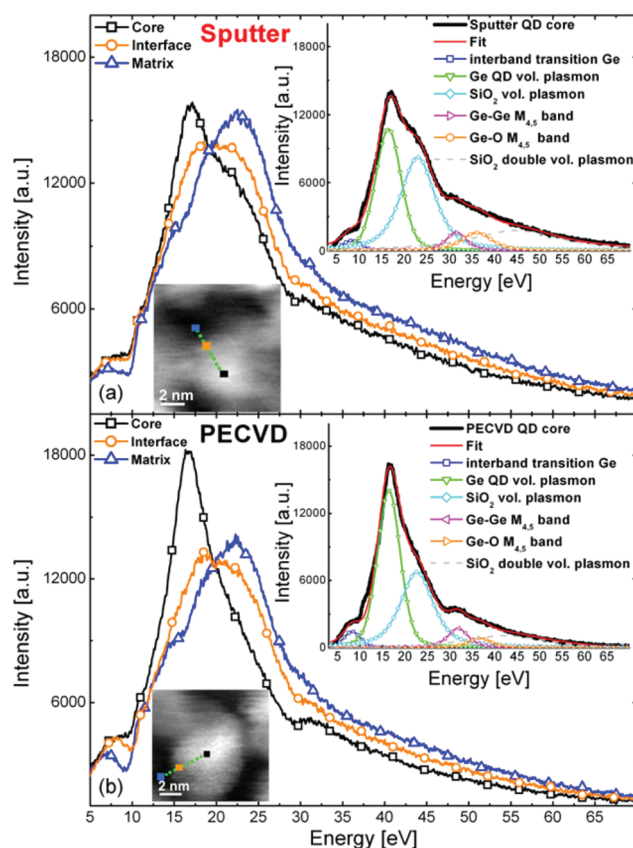


**Fig. 2** Low-loss EELS spectra in the core, interface and matrix region of Ge QD in SiO<sub>2</sub> grown by sputtering (a) or PECVD (b). The STEM images in the insets show the typical line-scan acquisition and probed area in (a) and (b). The different components of the EELS spectra in the core region are fitted by using the Voigt function and are shown in the panel figures for the case of sputter (a) and PECVD (b) QD.

tion deterioration effect due to plasmon delocalization, which usually is in the 1–2 nm range.<sup>35</sup> As shown in the insets of Fig. 2, moving from the SiO<sub>2</sub> matrix to the QD core region results in a clear modification of the EELS spectra. This is a direct signature of the different chemical contributions around the QD that are probed by the electron beam. In fact, the overall EELS spectrum contains several contributions coming from the plasmonic excitation of Ge, surrounding the SiO<sub>2</sub> matrix and Ge oxide states.<sup>36,36</sup> In particular, the two main components are related to the volume plasmon of the Ge QD (centered at 16–17 eV) and the excitation of the volume plasmon of the SiO<sub>2</sub> matrix (23–25 eV). The latter component gives another broad contribution peaked at around 46 eV due to the double plasmon loss in SiO<sub>2</sub>.<sup>37</sup> The remaining components are related to the inter-band transitions of the Ge–SiO<sub>2</sub> hetero-structure (5–10 eV range) and to the broad M<sub>4,5</sub> ionization edge of Ge QD, starting at around 29 eV. This latter contribution gives important information on the chemical arrangement at the interface of Ge QDs. In order to obtain a quantitative estimation of these features, the different components of the spectra were deconvoluted through Voigt fitting (see insets in both panels). Since our EELS spectra contain several contributions, we chose fixed values of the peak and FWHM of the different contributions, in accordance with the values reported in the literature. Therefore, the only free fitting parameter is the area of the different peak contributions, while the overall fitting inaccuracy is <5% (see Fig. 2S and 3S in the ESI†). From a closer comparison of the EELS spectra in the core region of the sputter [panel in Fig. 2(a)] and PECVD [panel in Fig. 2(b)] samples, different features are clearly visible, as a lower contribution of SiO<sub>2</sub> volume plasmon appears for the latter. Moreover, both sputter and PECVD QD spectra denote the presence of a broad peak centered at around 36 eV related to Ge-oxide (GeO<sub>x</sub>, x ≤ 2) species.<sup>38</sup> Indeed, the sputter film seems affected by a larger fraction of GeO<sub>x</sub> species with respect to the PECVD one. In fact, given the areas of Ge–O contribution ( $A_{\text{Ge-O}}$ ), the Ge–Ge M<sub>4,5</sub> band ( $A_{\text{Ge-Ge}}$ ) and the Ge volume plasmon peak ( $A_{\text{Ge-pl}}$ ), the amount of Ge-oxide species [here quantified as:  $F_{\text{Ge-O}} = A_{\text{Ge-O}} * (A_{\text{Ge-Ge}} + A_{\text{Ge-pl}})^{-1}$ ] for the sputter sample ( $F_{\text{Ge-O}}^{\text{sputter}} \sim 16 \pm 2\%$ ) appears to be twice that for the PECVD one ( $F_{\text{Ge-O}}^{\text{PECVD}} \sim 8 \pm 1\%$ ). The consistency of this behavior was systematically evidenced in several QD regions through Voigt fitting, which verified the presence of larger Ge–O peaks in sputter QDs with respect to PECVD ones (see Fig. 2S and 3S in the ESI†). Such a result evidences chemically different interfaces among PECVD and sputter QDs, with a relatively large amount of Ge-oxide states in the latter.

In order to give more insight into the structural arrangement around the QD interface, we performed line-scan acquisitions of the Z-contrast signal of high resolution HAADF STEM micrographs of Ge QDs in SiO<sub>2</sub> with size in the 3–7 nm range. The intensity of the HAADF signal mainly depends on the atomic number, Z, of the observed atomic species. Therefore, by considering the intensity of the Z-contrast signal across the QD diameter, it is possible to get reliable results on

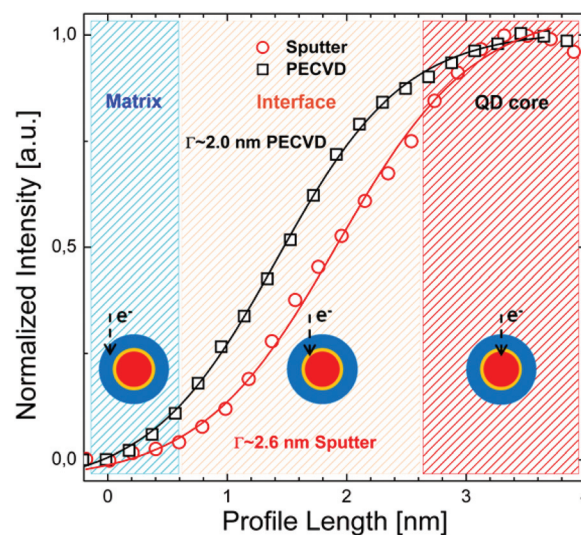
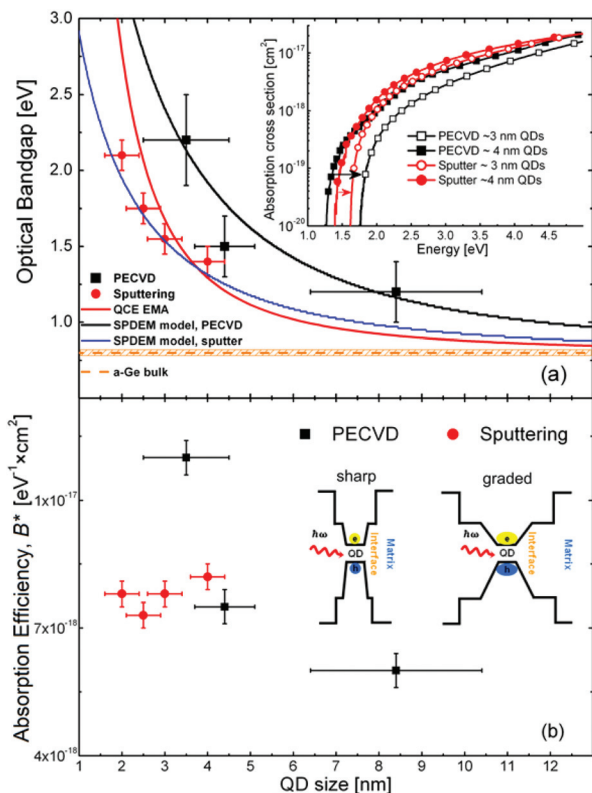


Fig. 3 Profile length of the Z-contrast signal across the diameter of ~3.5 nm sputter and PECVD Ge QDs. A schematic of the different regions probed by using the scanning electron beam is reported.

the interface thickness of our Ge QDs in SiO<sub>2</sub>. Fig. 3 shows the typical profile length of the Z-contrast signal obtained from the matrix to the core region of two sputter and PECVD Ge QDs of ~3.5 nm size (QD evidenced with D and B letters in Fig. 1S of the ESI†). The intensity of the Z-contrast signal increases with a characteristic length  $\Gamma$ , while moving from the matrix to the core region of the QD. This increase contains a “sphere-shape” contribution (coming from the shape-dependent SiO<sub>2</sub> thickness around the QD that is probed by the scanning electron beam, as shown in Fig. 3) and the intrinsic thickness of the interface shell. Given that the QD diameter is about 3.5 nm for both samples,  $\Gamma$  is expected to be at least as large as half the diameter, for the “shape” contribution, with the exceeding portion ascribable to the interface thickness. By fitting the SiO<sub>2</sub> plasmon-loss signals with sigmoid functions ( $f(x) = (1 + e^{-(x-x_0)/\Gamma})^{-1}$ , where  $x_0$  represents the point of inflection of the sigmoid function and  $\Gamma$  the characteristic length of the function increase), we estimated  $\Gamma$  of  $2.6 \pm 0.1$  nm for the sputter and  $2.0 \pm 0.1$  nm for the PECVD sample. These values point out that a fairly sharp interface can be assumed only for the PECVD case, while a thicker shell made of a larger contribution of oxides is evidenced for the sputter sample. Such behavior was observed for all the investigated QDs in our analysis (see Fig. 4S and 5S in the ESI†). The different interface shells, experimentally observed by STEM-EELS analysis on several investigated QDs, should be considered as an average difference present between the sputter and the PECVD Ge QD. Therefore, high resolution STEM-EELS technique demonstrated a chemical and a physical difference in the QD–matrix interface among sputter and PECVD Ge QDs, with the first ones thicker and richer in Ge-oxides than the latter ones. The presence of such an interface shell and its variation with the synthesis technique, in terms



**Fig. 4** Size variation of the optical bandgap (a) and absorption efficiency,  $B^*$  (b) of Ge QDs in  $\text{SiO}_2$  synthesized by sputtering and PECVD techniques. In (a) the red curve represents the standard EMA model of  $E_g$  for Ge QDs in  $\text{SiO}_2$ .<sup>44</sup> The black and blue solid lines represent the theoretical trend of  $E_g$  considering the correction of the SPDEM into the EMA model<sup>43</sup> and the different (sharp or graded) interface confining potentials, as drawn in the inset.

of thickness and stoichiometric oxide quality, is of utmost importance for the strength of carrier confinement occurring in nanostructures.

For these reasons, we studied the light absorption of Ge QDs in  $\text{SiO}_2$  to investigate if, and to what extent, the observed interface difference between sputter and PECVD samples can influence the strength of QCE. We evaluated the experimental absorption cross section from direct optical transmission and reflectance spectra of Ge QD films, as discussed in detail in ref. 4, 16. The absorption cross section gives the probability of photon absorption normalized by the Ge content,<sup>20</sup> thus representing an intrinsic property to be compared among different samples. Fig. 4 describes the competition between quantum confinement and interface effects occurring in the light absorption process of Ge QDs synthesized with different techniques. The inset of Fig. 4(a) shows the spectra of absorption cross section for sputter and PECVD films with different sizes of Ge QDs. A clear size-dependent shift of the absorption edge due to QCE is observed for both sets of samples. However, a different size-dependent shift of the absorption edge also appears, with PECVD QDs exhibiting a larger blue-shift than sputter QDs. These results indicate that the light absorption of

these systems is not set by the size only and may be largely influenced by the interface. When the interface is sharp enough a stronger role of QCE is expected, as we observed.

Indeed, the absorption cross section is closely connected to the optical bandgap  $E_g$  and the oscillator strength  $O_s$  of  $k$ -allowed transitions in the Brillouin zone (BZ) through formula (1):<sup>39,40</sup>

$$\sigma(\omega) = \frac{4\pi^2 e^2}{nc\mu_0^2 \rho \omega} |O_s|^2 \int_{\text{BZ}} \frac{2dk}{(2\pi)^3} \delta(E_c - E_v - \hbar\omega) \quad (1)$$

where  $\rho$  is the concentration of absorbing centers,  $n$  is the refractive index of the material,  $\mu_0$  is the exciton EM, while the integral represents the joint density of states (JDOS) in valence and conduction bands involved in the absorption of a photon with energy  $\hbar\omega = E_c - E_v = E_g$ . According to the Tauc formalism, under the hypothesis of parabolic band edges and optical inter-band transitions between quasi-localized states eqn (1) can be rewritten as:  $\sigma = \frac{B^*}{\hbar\omega} (\hbar\omega - E_g)^2$ .<sup>41</sup> Tauc coefficient,  $B^*$ , is directly proportional to the oscillator strength of the optical transition,  $O_s$ , and thus represents an estimation of the efficiency of light absorption.<sup>42</sup> Thus, it is possible to reliably determine  $E_g$  and  $O_s$  of nanostructures directly from their absorption cross section  $\sigma$ , as extensively discussed in ref. 4, 41, 43. We employed this analysis to experimentally measure  $E_g$  and absorption efficiency of our Ge QDs.

Fig. 4(a) shows the experimental values of  $E_g$  for Ge QDs, revealing a different behavior between the two sets of samples. In fact, PECVD QDs show a larger tuning of  $E_g$  with QD size, while a reduced energy dispersion appears for sputtered QDs. Moreover, the experimental tuning of  $E_g$  is not in good agreement with the standard EMA model [ $E_g(D) = E_g^{\text{bulk}} + A/D^2$ , where  $A$  is the confinement parameter  $A = \pi\hbar^2/2\mu_0 = 7.88$  eV  $\text{nm}^2$ ; ref. 43], which actually does not fit into any of the two data series [Fig. 4(a)]. This result is a direct consequence of the different interfaces observed by EELS analysis between the two types of QDs. In fact, the EMA model is usually used to describe carrier confinement in sharp and square-like potential barrier systems, considering bulk values of EM and neglecting any effect caused by a spatially-graded confinement potential  $V_c(x)$ , typical in the case of an interface shell between the QD and the matrix. In order to describe the effect of the interface, we developed a correction to the EMA model through a spatially dependent effective mass (SPDEM) formalism.<sup>26,45</sup> The SPDEM model is directly related to the potential  $V_c(x)$  for confined carriers and describes the effect of  $V_c$  on the EM, through the dispersion relationship:

$$E_g(D) = E_g^{\text{bulk}} + \frac{3\hbar}{\mu(D)\sqrt{2D}} \left[ \sqrt{\frac{V_{c,e}}{m_{c,e}^*}} + \sqrt{\frac{V_{c,h}}{m_{c,h}^*}} \right] \quad (2)$$

where  $\mu(D)$  is the renormalized SPDEM of excitons, having a dimensional dependence like  $\mu(D) = \mu_0 \epsilon_{\text{SPDEM}} D * [1 + (aD^2 + bD + c)^{-1}]$ .<sup>26,43</sup> The inclusion of the SPDEM into the EMA model gives better agreement between the theory and the experiment, as shown in Fig. 4(a). In particular,  $V_{c,e}$  and  $V_{c,h}$

were determined as fitting parameters in ref. 43, assuming QD interfaces were mostly composed of GeO<sub>2</sub> and GeO in the case of PECVD and sputter QDs, respectively. We found a larger interface potential for PECVD QD ( $V_{c,e}^{\text{PECVD}} \sim 1.1$  eV,  $V_{c,h}^{\text{PECVD}} \sim 3.3$  eV) with respect to sputtered ones ( $V_{c,e}^{\text{sputter}} \sim 0.9$  eV,  $V_{c,h}^{\text{sputter}} \sim 2.8$  eV). Moreover, it should be noticed that the potential offset extracted from the fit of PECVD QDs is close to the energy offset between Ge/GeO<sub>2</sub> ( $V_{0,e} = 1.2$  eV and  $V_{0,h} = 3.6$  eV),<sup>46</sup> confirming the higher Ge-oxide quality already indicated by the EELS analysis. Moreover, a sharp interface potential is correlated with a larger reduction in the EM, which gives rise to an increased energy dispersion through eqn (2). Therefore, PECVD QDs are closer to an ideal-like system, with a very sharp interface mostly composed of a GeO<sub>2</sub> shell between Ge QD and the SiO<sub>2</sub> matrix. On the other hand, sputter QDs suffer from a thicker interface with a more complex contribution of sub-stoichiometric Ge-oxide states that give rise to a graded interface, as schematically drawn in the inset of Fig. 4. While a sharp interface allows a large tuning of  $E_g$  through an effective exciton confinement and EM reduction, a spatially-graded interface gives rise to a weaker confinement effect. This evidence points out the paramount role of the interface in modifying the carrier confinement in nanostructures.

Finally, the effect of the interface in the quantum confinement of Ge QD is also visible in the trend of the Tauc coefficient  $B^*$ . This quantity is directly proportional to the oscillator strength  $O_s$  of light absorption through eqn (1).<sup>40</sup> In particular,  $O_s$  is strictly connected to the confinement of excitons through the exciton envelope function,  $G_{nm}(k)$ , and the optical matrix element,  $P_{nm}(k)$ , according to the formula:<sup>47,48</sup>

$$O_s = \frac{2}{\mu E_g} \left| \sum_k G_{nm}(k) \hat{x} \cdot P_{nm}(k) \right|^2 \quad (3)$$

The increase of the oscillator strength is usually observed, both experimentally and theoretically, in highly confined systems having a dimension smaller than the exciton Bohr radius.<sup>9,47,48</sup> This effect is often explained only as a consequence of the increased electron–hole overlap  $G_{nm}$  when the spatial dimension of the system is reduced. Our comparison between the sputter and PECVD Ge QDs illustrates two systems whose size variation is in the same range of 2–10 nm. Thus, we should expect quite a similar  $G_{nm}$  factor for both types of QDs and, consequently, a similar trend for the variation of  $O_s$ . However, this is clearly not the case.

Fig. 4(b) shows the size-dependent variation of  $B^*$  for PECVD and sputtered QDs. While PECVD QDs show an increased absorption efficiency for very strong spatial confinement, a fairly constant  $B^*$  appears in sputtered samples over the same size range. The different behavior observed for our systems suggests that other factors must be considered. Indeed, the variation of the reduced EM ( $\mu$ ) on the spatial dependence of  $O_s$  has to be considered. The better Ge-oxide quality and higher interface confinement potential in PECVD QDs yield a larger reduction in the reduced EM, which gives rise to an enhanced  $O_s$ , according to eqn (3), and therefore to

the increased  $B^*$  observed in Fig. 4(b). In contrast, the different behavior found for sputter QDs is a consequence of their interface quality. The thicker and poorer the Ge-oxide quality at the interface, the weaker the exciton confinement is. This effect gives rise not only to a reduced confinement for what affects the energy dispersion relationship, but also to anomalous size-independent oscillator strength. Therefore, the role of the interface is a key factor in the optical behavior of nanostructures. This is fundamental not only for a full understanding of the QCE in nanostructures, but also for exploiting their optical properties through both the control of size and interface engineering.

## Conclusions

In conclusion, we reported an exhaustive investigation on the role of the interface with respect to the quantum confinement effects occurring in Ge QDs. Closely packed arrays of 2–10 nm diameter Ge QDs in SiO<sub>2</sub> were produced by sputter and PECVD techniques. The structural quality and chemical composition of QD interfaces were investigated by extensive EELS analysis, which reveals a different interface in the two samples. In particular, a sharper and better quality interface was found for PECVD QDs, while sputtered QDs are characterized by a thicker interface shell containing twice the contribution of Ge-oxide states with respect to PECVD. Such a chemical and structural difference in the interface is the basis behind the different optical behaviour exhibited by Ge QDs. In fact, a large size-dependent tuning of both bandgap and optical oscillator strength is found for PECVD QDs. In contrast, sputter QDs exhibit a size-independent oscillator strength and only a moderate tuning of the bandgap. These differences were successfully explained by using a spatially dependent effective mass model, which accounts for the effect of the interface potential on exciton confinement. These results provide a new understanding of the role of interfaces on the quantum confinement effects in nanostructures. Moreover, our results indicate a further direction for an optimized exploitation of confinement effects in future nanostructure-based devices: not only by exploiting size effects, but also taking advantage of interface engineering.

## Acknowledgements

A special acknowledgement for this work goes to the memory of Dr Emel Sungur Ozen and to her unforgettable kindness. This work was sponsored by bilateral CNR-TUBITAK project “Application of nanoporous Si and Ge nanostructures to advanced solar cells” (grant no: 211T142) and in the framework of the project ENERGETIC PON00355\_3391233. Part of this work was performed at BeyondNano CNR-IMM, Italy, supported by MIUR under the project Beyond-Nano (PON a3\_00363). The authors thank C. Percolla, S. Tati and G. Panté (MATIS CNR-IMM) for expert technical assistance.

## References

- 1 F. Priolo, T. Gregorkiewicz, M. Galli and T. F. Krauss, *Nat. Nanotechnol.*, 2014, **9**, 19.
- 2 N. Usami, W. Pan, T. Tayagaki, S. Chu, J. Li, T. Feng, Y. Hoshi and T. Kiguchi, *Nanotechnology*, 2012, **23**, 185401.
- 3 S. Guha, J. Yang and B. Yan, *Sol. Energy Mater. Sol. Cells*, 2013, **119**, 1–11.
- 4 S. Cosentino, E. G. Barbagiovanni, I. Crupi, M. Miritello, G. Nicotra, C. Spinella, D. Pacifici, S. Mirabella and A. Terrasi, *Sol. Energy Mater. Sol. Cells*, 2015, **135**, 22–28.
- 5 X. Liu, X. Ji, M. Liu, N. Liu, Z. Tao, Q. Dai, L. Wei, C. Li, X. Zhang and B. Wang, *ACS Appl. Mater. Interfaces*, 2015, **7**, 2452–2458.
- 6 C. Y. Chien, W. T. Lai, Y. J. Chang, C. C. Wang, M. H. Kuo and P. W. Li, *Nanoscale*, 2014, **6**, 5303–5308.
- 7 Y. Kuo, Y. K. Lee, Y. Ge, S. Ren, J. E. Roth, T. I. Kamins, D. A. B. Miller and J. S. Harris, *Nature*, 2005, **437**, 1134–1136.
- 8 J. Liu, M. Beals, A. Pomerene, S. Bernardis, R. Sun, J. Cheng, L. C. Kimerling and J. Michel, *Nat. Photonics*, 2008, **2**, 433–437.
- 9 A. D. Yoffe, *Adv. Phys.*, 2002, **51**, 799.
- 10 N. Park, C. Choi, T. Y. Seong and S. Park, *Phys. Rev. Lett.*, 2001, **86**, 1355.
- 11 Z. H. Lu, D. J. Lockwood and J. M. Biribeu, *Nature*, 1995, **258**, 378.
- 12 Y. M. Niquet, G. Allan, C. Delerue and M. Lannoo, *Appl. Phys. Lett.*, 2000, **77**, 1182.
- 13 J. Heitmann, F. Muller, M. Zacharias and U. Gosele, *Adv. Mater.*, 2005, **17**, 795.
- 14 D. Mariotti, S. Mitra and V. Svrcek, *Nanoscale*, 2013, **5**, 1385.
- 15 M.-F. Ng and R. Q. Zhang, *J. Phys. Chem. B*, 2006, **110**, 21528.
- 16 S. Mirabella, R. Agosta, G. Franzò, I. Crupi, M. Miritello, R. Lo Savio, M. A. Di Stefano, S. Di Marco, F. Simone and A. Terrasi, *J. Appl. Phys.*, 2009, **106**, 103505.
- 17 R. Guerra, M. Marsili, O. Pulci and S. Ossicini, *Phys. Rev. B: Condens. Matter*, 2011, **84**, 075342.
- 18 P. B. Sorokin, P. V. Avramov, L. A. Chernozatonskii, D. G. Fedorov and S. G. Ovchinnikov, *J. Phys. Chem. A*, 2008, **112**, 9955.
- 19 G. Franzò, M. Miritello, S. Boninelli, R. Lo Savio, M. G. Grimaldi, F. Priolo, F. Iacona, C. Spinella and S. Coffa, *J. Appl. Phys.*, 2008, **104**, 094306.
- 20 S. Mirabella, S. Cosentino, A. Gentile, G. Nicotra, N. Piluso, L. V. Mercaldo, F. Simone, C. Spinella and A. Terrasi, *Appl. Phys. Lett.*, 2012, **101**, 011911.
- 21 R. Ghosh, P. K. Giri, K. Imakita and M. Fuji, *Nanotechnology*, 2014, **25**, 045703.
- 22 S. Takeoka, M. Fuji, S. Hayashi and K. Yamamoto, *Phys. Rev. B: Condens. Matter*, 1998, **58**, 7921.
- 23 M. Zacharias and P. M. Fauchet, *Appl. Phys. Lett.*, 1997, **71**, 380.
- 24 C. Bostedt, T. van Buuren, T. M. Willey, N. Franco, L. J. Terminello, C. Heske and T. Moller, *Appl. Phys. Lett.*, 2004, **84**, 4056.
- 25 S. Cosentino, E. Sungur Ozen, R. Raciti, A. M. Mio, G. Nicotra, F. Simone, R. Turan, A. Terrasi, A. Aydinli and S. Mirabella, *J. Appl. Phys.*, 2014, **115**, 043103.
- 26 E. G. Barbagiovanni, D. J. Lockwood, P. J. Simpson and L. V. Goncharova, *Appl. Phys. Rev.*, 2014, **1**, 011302.
- 27 S. Cosentino, S. Mirabella, M. Miritello, G. Nicotra, R. Lo Savio, F. Simone, C. Spinella and A. Terrasi, *Nanoscale Res. Lett.*, 2011, **6**, 135.
- 28 E. G. Barbagiovanni, D. J. Lockwood, N. L. Rowell, R. N. Costa Filho, I. Berbezier, G. Amiard, L. Favre, A. Ronda, M. Faustini and D. Grosso, *J. Appl. Phys.*, 2014, **115**, 044311.
- 29 A. Eljarrat, L. Lopez-Conesa, J. Lopez-Vidrier, S. Hernandez, B. Garrido, C. Magen, F. Peiro and S. Estrade, *Nanoscale*, 2014, **6**, 14971–14983.
- 30 M. H. Gass, A. J. Papworth, R. Beanland, T. J. Bullough and P. R. Chalker, *Phys. Rev. B: Condens. Matter*, 2006, **73**, 035312.
- 31 F. Gao, M. A. Green, G. Conibeer, E. C. Cho, Y. D. Huang, I. Perez-Wurfl and C. Flynn, *Nanotechnology*, 2008, **19**, 455611.
- 32 B. Zhang, S. Shrestha, M. A. Green and G. Conibeer, *Appl. Phys. Lett.*, 2010, **96**, 261901.
- 33 S. Cosentino, S. Knebel, S. Mirabella, M. Miritello, S. Gibilisco, F. Simone, A. Terrasi, H. Bracht and G. Wilde, *Appl. Phys. A: Solid Surf.*, 2014, **116**, 233–241.
- 34 T. Malis, S. C. Cheng and R. F. Egerton, *J. Electron. Microsc. Tech.*, 1988, **8**, 193–200.
- 35 P. Cuony, D. T. L. Alexander, I. Perez-Wurfl, M. Despeisse, G. Bugnon, M. Boccard, T. Soderstrom, A. Hessler-Wyser, C. Hebert and C. Ballif, *Adv. Mater.*, 2012, **24**, 1182–1186.
- 36 P. D. Nguyen, D. M. Kepaptsoglou, R. Erni, Q. M. Ramasse and A. Olsen, *Phys. Rev. B: Condens. Matter*, 2012, **86**, 245316.
- 37 K. Sasaki, S. Tsukimoto, M. Konno, T. Kamino and H. Saka, *J. Microsc.*, 2001, **203**, 12.
- 38 N. Jiang, J. Qiu and J. C. H. Spence, *Appl. Phys. Lett.*, 2005, **86**, 143112.
- 39 F. Bassani and G. Pastori Parravicini, *Electronic States and Optical Transitions in Solids*, ed. R. A. Ballinger, Pergamon Press, Oxford, 1975.
- 40 P. Y. Yu and M. Cardona, *Fundamentals of Semiconductors*, Springer, 4th edn, 2010.
- 41 J. Tauc, *Amorphous and liquid semiconductors*, ed. J. Tauc, Plenum Press, London and New York, 1974, p. 175.
- 42 S. Cosentino, M. Miritello, I. Crupi, G. Nicotra, F. Simone, C. Spinella, A. Terrasi and S. Mirabella, *Nanoscale Res. Lett.*, 2013, **8**, 128.
- 43 E. G. Barbagiovanni, S. Cosentino, A. Terrasi, S. Mirabella, D. J. Lockwood and R. N. Costa Filho, *J. Appl. Phys.*, 2015, **117**, 154304.
- 44 E. G. Barbagiovanni, D. J. Lockwood, P. J. Simpson and L. V. Goncharova, *J. Appl. Phys.*, 2012, **111**, 034307.

- 45 E. G. Barbagiovanni and R. N. Costa Filho, *Physica E*, 2014, **63**, 14–20.
- 46 M. Kobayashi, G. Thareja, M. Ishibashi, Y. Sun, P. Griffin, J. McVittie, P. Pianetta, K. Saraswat and Y. Nishi, *J. Appl. Phys.*, 2009, **106**, 104117.
- 47 W. T. Masselink, P. J. Pearah, J. Klem, C. K. Peng, H. Morkoc, G. D. Sanders and Y. Chang, *Phys. Rev. B: Condens. Matter*, 1985, **32**, 8027.
- 48 G. W. Bryant, *Phys. Rev B: Condens. Matter*, 1988, **37**, 8763.